NJC

PAPER

View Article Online
View Journal | View Issue

Cite this: *New J. Chem.*, 2016, **40**, 1420

Biogenic approaches using citrus extracts for the synthesis of metal nanoparticles: the role of flavonoids in gold reduction and stabilization†

Jelver Alexander Sierra,[a] Caio Raphael Vanoni,[a] Milton André Tumelero,[b] Cristiani Campos Plá Cid,[b] Ricardo Faccio,[c] Dante Ferreira Franceschini,[d] Tânia Beatriz Creczynski-Pasa[a] and André Avelino Pasa‡*[b]

Received (in Nottingham, UK) 10th August 2015,
Accepted 15th November 2015

DOI: 10.1039/c5nj02128f

www.rsc.org/njc

Synthesis of nanoparticles free from toxic chemicals and solvents is highly seen for large-scale production processes, particularly for use in biomedical/biotechnological applications. So far, although several methods for synthesis of metal nanoparticles using citrus extracts have been described, none of them clarify which compounds are responsible for both reduction and stabilization of NPs. Here we report the role of citrus flavonoids, hesperidin, hesperetin, rutin, naringenin, quercetin and diosmin, in the synthesis of gold nanoparticles (AuNP) at room temperature. Only in the presence of the citrus flavonoids, diosmin (Dm), and hesperetin (Ht), the reduction of $HAuCl_4$ in concentrations as high as 7 mM under alkaline conditions yielded concentrated and self-stabilized suspensions of uniform spherical nanoparticles with a narrow size distribution. We went further and focused on Ht, the most abundant flavonoid aglycone from citrus fruits known for its medicinal properties. HtAuNPs were characterized using high-resolution transmission electron microscopy, dynamic light scattering, X-ray photoelectron spectrometry and UV-Vis spectrophotometry. The NPs remained stable for months without significant changes in their shape and optical properties. Theoretical calculations using density functional theory were used to identify the functional groups involved in the electron transfer from the Ht molecules to gold, which seems to be the consequence of an initial complexation, leading to the reduction of Au^{3+} ions into Au^0. Besides, this procedure provides a one-pot method, showing potential for large-scale.

Introduction

Due to their distinctive catalytic and optical properties compared to bulk material, metal nanoparticles have attracted great attention to date in multidisciplinary research fields, such electronics,[1] catalysis,[2] environmental,[3] biomedical,[4] pharmaceutical,[5] textile[6] and cosmetic,[7] which suggest likely growth in commercial interest, calling for effective synthesis methods to match the increasing demand on AuNPs.

Several studies have indicated that the particle size, morphology and inter-particle interaction, as well as interactions between surface atoms and stabilizing ligands in metal nanoparticles are strong influencing factors on particle stability, and on optical, electrochemical, and biochemical properties,[8] which are critical for their final application and must therefore be assessed and rigorously controlled.[9] Such requirements justify the various on-going studies to develop or improve existing methods to synthesize stable AuNPs.

Avoiding processes with toxic chemicals and solvents is an important criterion for green approaches to nanoparticle synthesis, supporting also the idea of subsequent use in biomedical applications. In contrast to other chemical methods that cause the adsorption of some toxic chemical species on the particle surface, Turkevich *et al.*[10] developed a low cost procedure with reaction occurring in water as the solvent, and low pollution potential by pouring a measured amount of sodium citrate into a boiling solution of up to 2.5 mmol L^{-1} of chloroauric acid $HAuCl_4$ at reflux to produce biocompatible AuNPs.[8] With this method the nanoparticles display a narrow distribution and can be easily handled in applications, with the drawback of aggregation when

[a] *Departamento de Ciências Farmacêuticas, Grupo de Estudo de Interações entre Macro e Micromoléculas, Universidade Federal de Santa Catarina, 88040-900-Florianopolis, Brazil*
[b] *Departamento de Física, Laboratório de Filmes Finos e Superfícies, Universidade Federal de Santa Catarina, 88040-900-Florianópolis, Brazil. E-mail: andre.pasa@ufsc.br; Fax: +55 48 3234 0599; Tel: +55 48 3234 0599*
[c] *Cryssmat-Lab and Centro NanoMat, Facultad de Química, Universidad de la República, Montevideo, Uruguay*
[d] *Instituto de Física, Universidade Federal Fluminense, Niteroi-RJ, Brazil*
† Electronic supplementary information (ESI) available. See DOI: 10.1039/c5nj02128f
‡ Departamento de Física, Campus Universitário–Trindade, P. O. Box, Caixa Postal 476 CEP: 88.040-900 - Florianópolis, SC, Brazil.

concentration procedures are attempted. Citrate reduction is by far the most frequently used method, and remained the leading approach to attend the growing demand for AuNPs.

Alternative methods relying on bioreduction by microorganisms, fungi, plant extracts, biomass or even fruit juices have also been developed and proven to be suitable for synthesizing metal NPs with different sizes and shapes.[11] Recently, several studies regarding citrus fruits and peel extracts mediated reduction of gold, copper and silver into nanoparticles have been reported,[12–22] as they are supposed to be non-toxic, simpler and cheaper when compared to most of the current techniques. In some of those studies, metal reduction and stabilization of NPs have been attributed to a wide range of phytochemicals (*i.e.* ascorbic and citric acids, terpenoids, flavonoids, quinones, phenolic acids, pectins, proteins, *etc.*), but none of them clearly established any proof of which compounds are in fact responsible. Even more, though the approach has proven successful, several abiotic factors (metabolite seasonality, circadian rhythm, developmental stage and age, temperature, water availability, UV radiation, soil nutrients, altitude, atmospheric composition and tissue damage) affect secondary metabolite production in plants and lead to a high quali- and quantitative variability in juices and extract composition,[23,24] which could be unfavorable to the reproducibility among batch runs. Accordingly, Prathna *et al.* suggested phytochemicals as a valid alternative in the biomimetic synthesis of gold nanoparticles.[25]

Hesperetin (Ht) belongs to the flavanone subclass of flavonoids, and its glycoside form hesperidin (Hd) is the predominant flavonoid in the peels of lemons and oranges. Along with other citrus flavonoids Ht displays important medicinal properties such as anti-inflammatory, antihypertensive, anti-atherogenic, antitumor, antifungal, antioxidant, and anti-allergic, shows neuroprotective and anti-depressive effects, and improves memory and learning.[26] Regardless of the high content of Ht, Hd and other compounds in citrus peels, this material is usually processed as a by-product or wasted. For this reason, one of us developed an optimized method to recover antioxidant flavonoids from citrus peels, offering a source of raw material that could be exploited.[27]

Concretely, this work offers important developments: firstly, a reproducible method following the principles of green chemistry for the synthesis of AuNPs using citrus flavonoids as reductants for $HAuCl_4$ in concentrations as high as 7 mM that can be used as an alternative to existent methods, with higher yields, was developed. Secondly, using Ht as the reductant and stabilizing agent adds value to a material frequently discarded, and gives spherical AuNPs, with narrow size distribution, stable for at least 1 year, with minimal aggregation. And finally, the visual/spectral properties, as well as, a theoretical calculation explaining the electron transfer from Ht hydroxyls to Au^{+3} through complexation, leading to Au^0 and also to the stabilization of the HtAuNPs are presented.

Experimental section

Materials

Hydrogen tetrachloroaurate trihydrate ($HAuCl_4 \cdot 3H_2O$, 99.9%), sodium hydroxide, diosmin (Dm), naringenin (Ng), hesperidin (Hd), rutin (Ru), quercetin (Qc) and hesperetin (Ht) were purchased from Sigma Aldrich (USA); Type I water was obtained from a Milli-Q water purification system (resistivity 18.2 MΩ). All glasswares were washed with aqua regia for the removal of potential artificial nucleation sites and rinsed three times with deionized water.

Synthesis of gold nanoparticles

The size of AuNPs is influenced by a number of factors such as pH, temperature, precursor/reducing agent ratio, and reactant concentrations. We chose to perform the synthesis at room temperature and because flavonoids precipitated in acidic medium dissolving only in alkali, a 2^k full factorial design varying just the concentration of reagents was set up. A measured volume of 38 mmol L^{-1} solution of $HAuCl_4$ was mixed at room temperature and under mild stirring with a flavonoid solution previously prepared in NaOH 0.1 mol L^{-1}, varying the molar ratio of gold:flavonoid and using a final volume as low as 1 mL. Colloidal suspensions were agitated for additional 30 min and stored at room temperature. The gold nanoparticle suspensions were purified by 2× centrifugation at 6000 × *g* for 7 min followed by dispersion of the pellet in deionized water.

In the design, the optimal conditions for the synthesis of the gold nanoparticles stabilized *in situ* by hesperetin were: $HAuCl_4$ and Ht 4 mmol L^{-1}, room temperature, 25 min and low agitation (200 rpm).

UV-Visible spectroscopy

The reduction of $HAuCl_4$ to AuNPs was monitored by measuring the UV-vis spectra of the solutions as prepared, in a picodrop spectrophotometer using polymer pippet tips of 1 mm optical path length at a resolution of 5 nm from 400 to 780 nm. Deionized water was used as blank. The recorded spectra were then re-plotted using Graphpad prism 5.0.

Particle size analysis and zeta potential measurements

The particle size and charge of the AuNP along with their polydispersity were determined as prepared and after purification using a Zetasizer Nano ZS (Malvern, UK) equipped with a 633 nm He–Ne laser beam, at 173° back-scattering angle. AuNPs surface charges (zeta potential) were determined by measuring their electrophoretic mobility at 25 °C. For calculations, monomodal acquisitions fitted according to the Smoluchowski equation were used. Each experiment was carried out with three replicates ($n = 3$) and the data are presented as mean ± standard deviation (SD).

Transmission electron microscopy

The shape and size of the particles were determined by transmission electron microscopy (TEM) using a JEOL JEM-2100 (200 KeV) microscope equipped with the selected area electron diffraction pattern (SAED). Samples were prepared by dipping Formvar-carbon copper grids (200 mesh) into a dilute suspension (1 : 1000) of Au nanoparticles for several seconds. The TEM grids were removed from the solution and allowed to dry in air. The size distributions of the AuNPs were determined from the

diameters of at least 100 particles from a representative region of the enlarged micrographs using ImageJ.[28]

X-ray photoelectron spectroscopy (XPS)

XPS experiments were performed in a Thermo Scientific ESCALAB 250xi spectrometer using monochromatic Al Kα radiation ($h\nu$ = 1486.6 eV). Films of purified AuNPs were prepared by casting a drop onto cleaned silicon wafers and then air-dried. The pressure on the spectrometer chamber was 7×10^{-9} mbar, and the analyzer pass energies were 100 and 25 eV for survey and narrow mode scans, respectively. Corrections for sample charge were made assuming a constant binding energy for the C 1s band at 285 eV. All peaks were fitted using Gaussian–Lorentzian curves (GL30) after the Shirley background removal in all spectra.

In vitro stability studies

Stability of the purified HtAuNPs over time (0, 12, and 24 months) was monitored using absorption spectroscopy. Their characteristic localized surface plasmon resonance LSPR band was checked for signs of agglomeration. The effect of dilution was also evaluated by stepwise addition of 0.1 mL of DI water to 0.1 mL of HtAuNPs and the subsequent absorption measurements.

Computational simulations

Density functional theory (DFT)[29,30] simulations using Gaussian 09[31] were performed using the hybrid exchange–correlation functional B3LYP;[32–34] the LAN2DZ basis set was selected for Au[35] and the 6-31+g(d,p) for the other atoms. No restrictions were applied to the point group symmetry of the molecules, allowing a full degree of freedom during the geometrical optimization selecting a force and total energy tolerance of 3×10^{-4} a.u. and 1×10^{-6} a.u., respectively. Vibrational analysis were performed in order to confirm that stable states of molecular systems correspond to global and local minima on their potential energy surfaces.

The relative stabilities of all clusters were determined by the corresponding formation energies (E_{form}) according to:

$$E_{form}\ (\text{eV}) = E_{Total} - (E_{Ht/Hc} + E_{Au+3}), \quad (1)$$

where E_{Total}, E_{Ht}, E_{Hc} and E_{Au+3} correspond to ground state total energy for the Au–Ht complex, Ht, hesperetin chalcone (Hc) and Au^{+3} single atom, respectively.

With the aim to simulate the experimental conditions, as similar as possible, the polarizable continuum model (PCM)[36] was selected to take into account the bulk solvent effects.

Excitation energies and oscillator strengths for the most stable geometries were obtained by means of time-dependent DFT (TDDFT)[37,38] calculations. Twenty transitions, singlet–singlet and triplet–triplet, were performed using the same exchange–correlation functional and basis set.

Results and discussion

Synthesis of gold nanoparticles

Citrus fruit juices and peel extracts have a complex composition and contain several compounds showing strong antioxidant and radical scavenging activities, flavonoids included. Since the antioxidant activity of a substance is usually directly correlated with its reducing capacity,[39] it is expected that electrons generated during the flavonoid oxidation reaction would reduce Au^{3+} ions to Au^0 atoms. Furthermore, several authors recently succeeded in synthetizing gold nanoparticles with different shapes and sizes using citrus juices.[12,13,19] These authors suggested that reduction could be ascribed to ascorbic and citric acids, and the capping to proteins present in the juices, although the contribution of other components could not be ruled out. Also Das *et al.*[40] recently reported the sonochemical synthesis of AuNPs using quercetin acting both as reducing and therapeutic agents.

It is generally accepted that flavonoid glycosides are water-soluble and their aglycone counterparts are usually less so. Tested flavonoids were practically insoluble in water and precipitated under acidic conditions; thus, they were solubilized in an alkaline media (NaOH 0.1 mol L^{-1} pH 11). Under these basic conditions the reduction potential of flavonoids shifts towards lower values (59 mV per pH unit), and also occurs the successive replacement of chlorine atoms of $HAuCl_4$ by hydroxyls leading to unstable intermediates [$AuCl_{4-n}(OH)^n$] that are expected to be easier to reduce.[41] We hypothesized that, given the higher standard reduction potential of the $Au^{3+}(aq)/Au^0$ pair (1450 mV *vs.* the standard hydrogen electrode, SHE) compared to that of Ht (470 mV), Dm (512 mV), Qc (330 mV), Ng (600 mV), Ru (400 mV), Hd (400 mV), gold reduction would be thermodynamically feasible.

In a first attempt to reduce $HAuCl_4$ using citrus flavonoids, the course of reaction was followed by a spectrophotometer for the appearance of the LSPR band characteristic of Au^0 nanostructures. Although Qc and Ru were able to reduce gold ions they did not effectively stabilize them, no AuNPs were formed by adding Hd and only Dm and Ht showed clearly defined narrow LSPR bands that suggest homogeneous AuNPs formation, see Fig. 1. Ht is by far the most abundant flavonoid aglycone in orange, and tangerine,[42] therefore it was a selected model for this work. A reagents blank ($HAuCl_4$ and NaOH) was left to react for 24 h at room temperature (25 °C), without the formation of gold nanoparticles, indicating that flavonoids were indeed responsible of reduction.

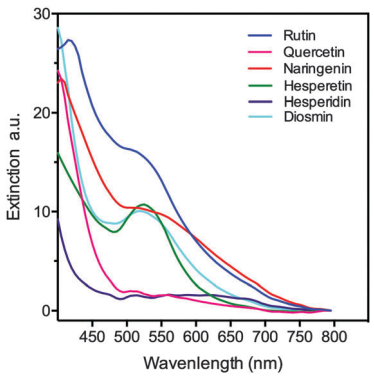

Fig. 1 Flavonoids diosmin and hesperetin reduce $HAuCl_4$ and yield self-stabilized gold nanoparticles. UV-Vis spectra of alkaline solutions of flavonoids (2 mmol L^{-1}) with the addition of chloroauric acid (2 mmol L^{-1}) recorded after 60 minutes of reaction.

For Ht, a different behavior was observed when the addition order of the reagents was altered as can be seen in Fig. 2. When $HAuCl_4$ was poured into an alkaline solution of flavonoid (type 1), a rapid formation of AuNPs was observed, perceived as transient solutions turning from black to gray, then to violet and finally to ruby red within 5 min. In contrast, the inverse process of adding the flavonoid solution over $HAuCl_4$ in NaOH proceeds slowly (type 2), reaching its end in about 30 min, although the color patterns of suspensions were preserved.

HtAuNPs exhibiting a localized surface plasmon resonance (LSPR) within 520–550 nm wavelength interval characteristic of gold colloid containing particles below 100 nm were produced.[43] The results obtained from both the processes are comparable to the findings of Mikhlin *et al.*[44] that found a series of transiently colored suspensions during the synthesis of gold nanoparticles with citrate, and these transitory colors were explained by the increasing interparticle distances within transient mesoscale intermediates, described as large aggregates of nanoparticles that progressively decreased in size. The type 2 reaction is studied thoroughly in this work.

Fig. 3a shows the UV-Vis spectra of gold nanoparticles produced by reducing $HAuCl_4$ with hesperetin at different concentrations (1, 4, and 7 mmol L^{-1}). As it can be seen, most samples showed maximum LSPR bands (λ_{max}) in the interval 520–530 without any peak in the near-IR region indicating the formation of spherical nanoparticles. An exception was samples prepared with gold in excess (4 : 1 and 7 : 1), that displayed very weak λ_{max} peaks, around 640 nm after synthesis, and the suspensions became unstable and precipitated after few minutes, spectra and size measurements were not recorded.

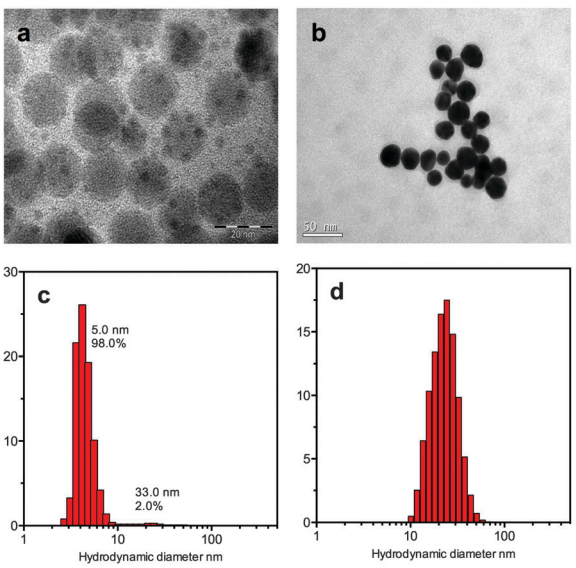

Fig. 2 (a) TEM image of type 1 HtAuNPs produced by adding $HAuCl_4$ over Ht, displaying two sizes, 3.5 and 15 nm and (b) TEM image of type 2 HtAuNPs produced by adding Ht over $HAuCl_4$, showing a homogeneous population of 15 nm. Size distribution of each HtAuNPs suspension was also measured by DLS; accordingly, in (c) type 1 HtAuNPs were polydisperse suspensions of 5 nm and 33 nm, while in (d) only one population of 32 nm was found for type 2 HtAuNPs.

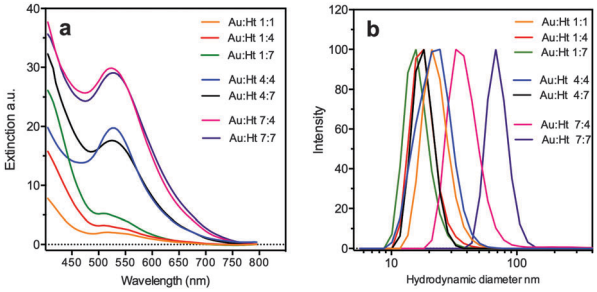

Fig. 3 Ht reduces efficiently $HAuCl_4$ and yields self-stabilized gold nanoparticles with hydrodynamic diameters up to 68 nm and SPR values in the range of 520–530 nm. (a) UV-Visible spectra of two-fold diluted gold nanoparticles formed by the addition of different concentrations of $HAuCl_4$ (1, 4, and 7 mmol L^{-1}) into alkaline solutions of Ht (1, 4, and 7 mmol L^{-1}) recorded after 60 minutes of reaction. (b) Size distribution measured by DLS.

Taking into account that the reaction mixture with a molar ratio of 1 and a concentration of 4 mmol L^{-1} yielded nanoparticle suspensions with adequate size and good distribution, particle growth was monitored over time recording optical absorption in the wavelength interval of 400–800 nm. In spectra plotted when the gold precursor was kept constant at 1 mmol L^{-1}, LSPR bands were located at around 520 nm, though few HtAuNPs were obtained. In contrast, the increase of the precursor and hesperetin concentration to 4 and 7 mmol L^{-1} enhanced the reaction rate and yielded more concentrated suspensions, but only at a molar ratio of 4 : 4 the LSPR band was 522 nm and showed the narrowest full width at half maximum (FWHM). DLS size distributions in Fig. 3b show that the hydrodynamic diameter varies considerably with the increase in reactant concentrations and the particle average hydrodynamic sizes were in the range of 14 to 68 nm. It is worth to note that in the reaction mixture gold : hesperetin of 7 : 4, gold was fully reduced (97%) and HtAuNPs stabilized, indicating the autocatalytic behavior of the reaction.

Fig. 4a shows a main maximum LPSR band (λ_{max}) appearing after 30 s at 630 nm and gradually shifting to blue increasing in intensity to reach a maximum at 522 nm. Although the reaction was left to continue up to 82 minutes, no important changes were observed in the position of the λ_{max} value after 30 minutes, and also the normalized absorbance value measured at 522 nm (A_{522}) reached its maximum within the same time frame. Even more, absorption at the longer wavelength of 650 nm (A_{650}), commonly regarded as an indicative of aggregates somewhat increased at first but then decreased with the time, as shown in Fig. 4b.

The total amount of elemental gold produced was determined by FAAS. The gold was fully reduced, and the concentration of gold on nanoparticles fell between 95–101% of the concentration originally used in the reaction mixtures (data not shown), demonstrating the efficient reduction of $HAuCl_4$ to elemental gold by Ht.

From the DLS measurements during HtAuNPs formation the hydrodynamic diameter (Z-average) was recorded. In Fig. 4c are displayed the time course of the hydrodynamic diameter and polydispersity index (PdI). Due to the fast onset of the reduction, analysis of the obtained curves only allowed the

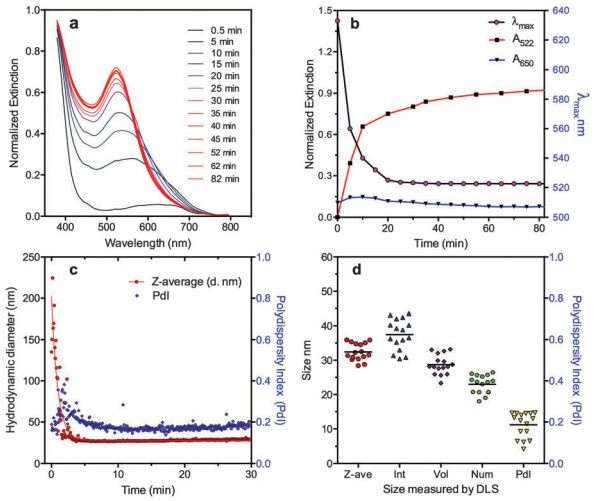

Fig. 4 HtAuNPs are synthetized within 30 minutes, starting with black colored suspensions formed by large aggregates that gradually decrease in size. The time course of the reaction at room temperature of a mixture of chloroauric acid and hesperetin at a molar ratio of 1 and a concentration of 4 mmol L^{-1} and pH 11 was monitored by (a) UV-Vis spectra after 0.5 min (black), 5 min (dark gray), 10 min (dark violet), 15 min (violet), 20 min (magenta), and 25 min and (ruby red). (b) Position (λ_{max}) of the main plasmon peak and absorbance at 522 and 650 nm. (c) Hydrodynamic diameter (Zeta-average) and polydispersity index measured, and (d) size of different batches of HtAuNPs measured by DLS.

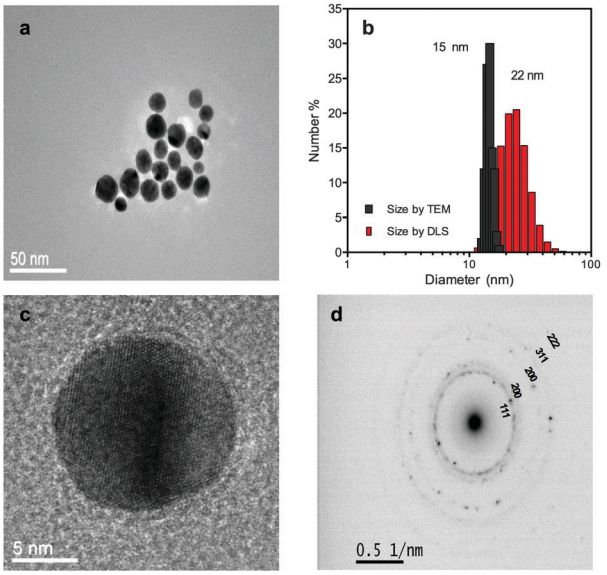

Fig. 5 Homogeneous suspensions of negatively charged crystalline HtAuNPs were synthetized by adding chloroauric acid to a hesperetin solution at a molar ratio of 1 and a concentration of 4 mmol L^{-1}. (a) TEM image of HtAuNP as prepared, (b) size distribution by a number of as-prepared HtAuNPs measured using DLS or diluted by TEM, (c) their high-resolution image, and (d) the SAED pattern.

differentiation of two stages of HtAuNPs formation, *i.e.*, nucleation and autocatalytic growth with no incubation period, which could be explained by the high concentration of the reactants, as previously discussed.[41] At the beginning of the reduction reaction DLS measurements detected large particles up to 250 nm in the black-colored suspensions, which decreased in size in less than 10 min, getting close to the size of HtAuNPs measured individually by TEM in the final colloidal suspensions. This behavior is in agreement with our findings with UV-Vis, thus colored suspensions could be explained by the presence of aggregates as reported by Mikhlin *et al.*,[44] who also found large scattering structures with an average hydrodynamic diameter of up to 125 nm in the initially colored suspensions produced by the citrate method.

Ideally a good and effective synthesis method to match the demand of NPs for any intended use should be highly reproducible. In Fig. 4d are plotted data of independent syntheses (n = 16). Results presented in this figure include the Z-average, Z-ave, and the mean diameter obtained from the size distributions weighted by intensity (Int) of the scattered radiation and also weighted by nanoparticles volume (Vol) and number (Num), along with the polydispersity index. As it can be seen, the method is highly reproducible, displaying coefficients of variation below 15% for the mean diameter.

The shape and size distribution weighted by the number of the HtAuNPs were determined by transmission electron microscopy (TEM). Fig. 5a shows a typical TEM image of HtAuNPs (diluted 1 : 1000), and their corresponding size distribution histogram is presented in Fig. 5b, and compared with the DLS results. It is evident from these figures and the high-resolution image in Fig. 5c that HtAuNPs are spherical in shape, well separated from each other and showing a narrow size distribution.

Several authors have pointed out that drying and storing the NPs on surfaces could cause changes that may not reflect accurately the nature of the sample in the liquid dispersion.[45] We have performed DLS measurements and compared with TEM results, for the same set of NPs. The histogram of the size distribution by the number in Fig. 5b has a normal distribution similar to the one obtained by TEM. The shift of the center to 22 nm for a PdI of 0.187 could be explained by assuming that DLS is measuring the gold core with a surface chemisorption of hesperetin and its oxidation products, whereas TEM is showing only the Au core. Is also possible that DLS due to its lower resolution only discriminates NPs with large sizes or aggregates made of 2 or more nanoparticles. Our data reproduces the report for 15 nm AuNPs by Mahl *et al.*[46]

The crystalline nature of HtAuNPs in Fig. 5c was further investigated by selected area electron diffraction (SAED) analysis. As can be seen from the SAED pattern in Fig. 5d of a selected area with many HtAuNPs, the nanoparticles are highly crystalline and electron diffraction rings could be assigned to (111), (200), (220), (311), and (222) planes of a face-centered cubic (fcc) metallic gold. Additionally, the interplanar distance measured in the high-resolution images of 2.35 nm corresponds to the fcc lattice parameter of (111) planes oriented in the 111 zone.

It is generally accepted that colloids showing a zeta potential outside the interval of −25 to +25 mV is stable and that agglomeration only occurs when the attraction between NPs exceeds the repulsive forces among them with a zeta potential approaching the point of zero charge.[47] HtAuNPs displayed a negatively charged layer of −44 mV that keep them separated

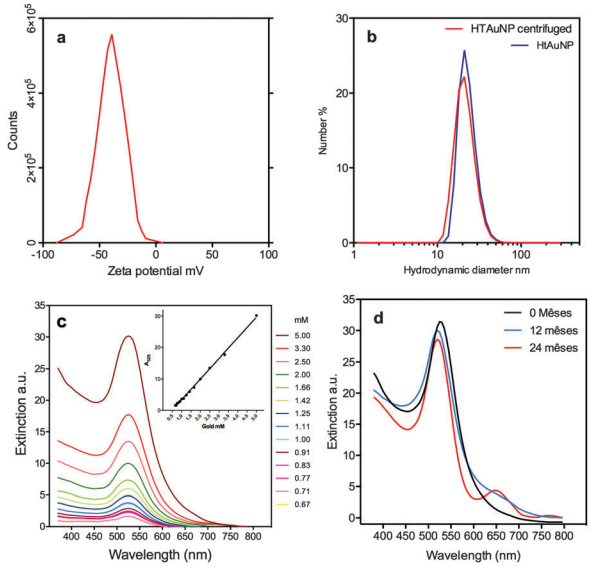

Fig. 6 UV-Vis spectra and DLS measurements of HtAuNPs purified by centrifugation over time. HtAuNPs are stable under conditions of (a) dilution, (b) centrifugation (2× 6000 × *g* 7 min), and (c) laboratory storage conditions (2–8 °C for 2 years).

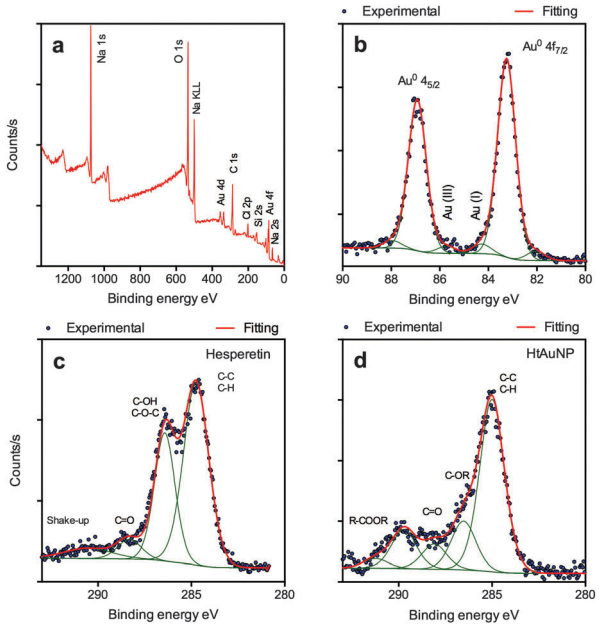

Fig. 7 XPS measurements: (a) XPS survey spectrum of the film formed by dropping and drying on silicon substrate hesperetin reduced and self-stabilized gold nanoparticles. (b) Au 4f, (c) Hesperetin C 1s, and (d) HtAuNPs C 1s envelopes deconvoluted into its components.

from each other, see Fig. 6a, and could explain the long-term stability of our colloids, which is longer than one year. Easy manipulation of nanoparticles on applications is highly desirable and centrifugation is a flexible method commonly used to purify nanoparticles after chemical modification.[48] HtAuNPs showed a stable size as measured by DLS after 2 centrifugation steps as shown in Fig. 6b. However aggregation was observed when 3 centrifugation steps were used (not shown). Also, in order to judge the degree of attraction and stabilization of Ht on HtAuNPs, a concentrated suspension was diluted stepwise and the UV-Vis spectra were recorded. As shown in Fig. 6c Ht is effective in the stabilization with the absorption showing a linear behaviour after dilution (inset). Finally, Fig. 6d shows the UV-Vis spectra of a purified suspension after 2 years of storage. HtAuNPs are fairly stable for at least one year, the 2 year spectrum showed an additional, well defined LSPR band at 650 nm indicating aggregation.

In their previous work, Ivanov *et al.*,[47,49] suggested that while both SPR and zeta potential data would provide important information regarding the composition, concentration and effective charge of nanomaterials, more precise information regarding the fine characterization of organic–inorganic interfaces should be gathered by using other techniques, such as X-ray photoelectron spectroscopy (XPS).

The XPS analyses of HtAuNPs are presented in Fig. 7. The survey spectrum of Fig. 7a shows peaks due to the presence of gold, carbon, oxygen, sodium, chlorine, and silicon. In spite of the careful purification of HtAuNPs, the detection of sodium and chlorine could be explained by the electrostatic interactions among negatively charged HtAuNPs and Na^+, and Cl^- counter-ions. The Au $4f_{7/2,5/2}$ coupled peaks in the narrow range of binding energy, displayed binding energies of 84.38 and 88.07 eV with a spin–orbit splitting of 3.68 eV and an area ratio of 0.75 that are in good agreement with the values found in the literature for pure metallic gold,[50] along with some minor contributions of Au^{1+} and Au^{3+}, indicating the O–Au bonding, as displayed in Fig. 7b.

The C 1s envelope for an Ht film and HtAuNPs deposited on Si is shown in Fig. 7c and d, respectively. In spectral analysis peaks C–C (285.2 eV), C–OR (286.6 eV), C═O (288.5 eV) characteristic of Ht were observed, noteworthily an additional peak typical of COOR (290.2 eV) was also observed, and could be attributed to Ht oxidation products. Although originally the COO-R moiety is not present in Ht, both the redox reaction and the organic–inorganic interaction on the metallic surface could have induced the molecule to rearrange its internal structure, leading to complex structural deformation and cleavage of the adsorbed molecules. Still, when a folin ciocalteau redox reaction was performed, 1.6 mmol L^{-1} of total polyphenol content was found on the HtAuNPs (equivalent to 40% of the original input). In the O 1s envelope (Fig. S1, ESI†), the oxygen atom is present in two chemical states, O singly bonded to carbon and O doubly bonded to carbon, the latter increasing in proportion, supporting the idea of oxidation products stabilizing the HtAuNPs surface and confirming the results seen in the carbon spectra.

Computational simulations

The purpose of performing the simulations was to understand the mechanism of the reduction of Au^{3+} ions as well as the surface capping mechanism. Accordingly, theoretical evidence for the Au^{+3}:Hesperetin and Au^{+3}:Hesperetin chalcone (Hc) interactions leading to the formation of gold nanoparticles simulating the experimental conditions as close as possible is provided. Firstly, the possible stable conformations of Ht in the

solvent were calculated. Then, all the possible ways in which Au^{3+} ions could interact with the molecule were studied, for that, the interactions between different Au : Ht/Hc ratios were evaluated, determining stable structural geometries. In all cases the total charge transfer between gold and Ht^{-3} and Hc^{-4} molecules was evaluated. Finally, time dependent density functional theory (TDDFT) calculations for the optical properties of the most relevant structures are presented.

Neutral Ht molecule. First, the behavior of Ht in the gas phase and solvent was compared using the Polarizable Continuum Model (PCM) calculations for the solvent. The Ht molecule is quite rigid with not many rotational bonds in the structure. The only difference between the two phases is the rotation of the phenyl group attached to the C ring resulting in two conformations (a) and (b) for the gas phase and PCM, respectively, as shown in Fig. S2 (ESI†). The dihedral angle Φ formed by O–C–C–C atoms (indicated in cyan in Fig. S2a, ESI†), has values -7.76° and 55.64° for the gas phase and PCM, respectively. Regarding the electronic structure, there are no important changes, since the HOMO–LUMO gap is 4.33 eV and 4.20 eV for gas and PCM, respectively.

Charged Ht molecules. It is well known that in aqueous alkaline solutions at pH = 11 Ht will be either as Ht^{-3} phenolate or as Ht chalcone (Hc^{-4}), as reported by Di Mauro *et al.*[51] by the opening of the C ring of Ht. Therefore, calculations also for Ht^{-3} in the gas phase and water and Hc^{-4} in water were also performed, and its optimized geometrical conformations are shown in Fig. S2c and S3e (ESI†).

The total energy and HOMO–LUMO gaps shown in Table S1 (ESI†) reveal the instability of Ht^{-3} in the gas phase (low gap energy). The Ht^{-3} (gas phase) structure displays a total energy considerably higher than the other molecules, even when differences arising from the use of PCM were considered. Therefore, PCM was included in all the following calculations.

Au^{+3} and Ht^{-3} interactions. The anionic form of Ht interacts with Au^{+3} at different proportions. In the first case, for 1 : 1 ratio, Au^{+3} is able to interact with a single oxygen atom in two sites of Ht, either on the A ring and with the oxygen atom of the deprotonated hydroxyl group on C_5 (system 1) or on the B ring, with the deprotonated hydroxyl located on C_3' (system 2). Once optimized, important changes were observed in both cases, as can be seen in Fig. 8. Due to the strong interaction with Au^{+3}, the Ht^{-3} molecule underwent an intramolecular reaction giving place to a final bicycle configuration, which is observed in the gas phase for both cases (1a) and (2a), but in solvent just for the structure (1b). In solvent, complex (2b) displays important conformational changes, without intramolecular reaction in the Ht molecule, but revealing non-real frequencies in its vibrational spectrum confirming its unstable nature. Yet, a charge transfer from the Ht^{-3} molecule to Au^{+3} was observed in all the cases. Before optimizations the starting charge of gold was +3, and after the optimization reached values approaching to zero, see Table 1. These values are quite close to those obtained by Singh *et al.*[52] for curcumin interacting with gold. Here, solvation effects stabilize the negative charge on Ht, limiting the amount of charge that is transferred to gold in the reduction, as observed in the net charge of gold atoms when comparing the gas phase and solvent calculations. Though formation energies in Table 1 would indicate a possible spontaneous process for Au:Ht interaction, still a direct comparison between structures is rather complex, since the energies corresponding to the intramolecular reaction and structural distortion of the Ht are included in those values.

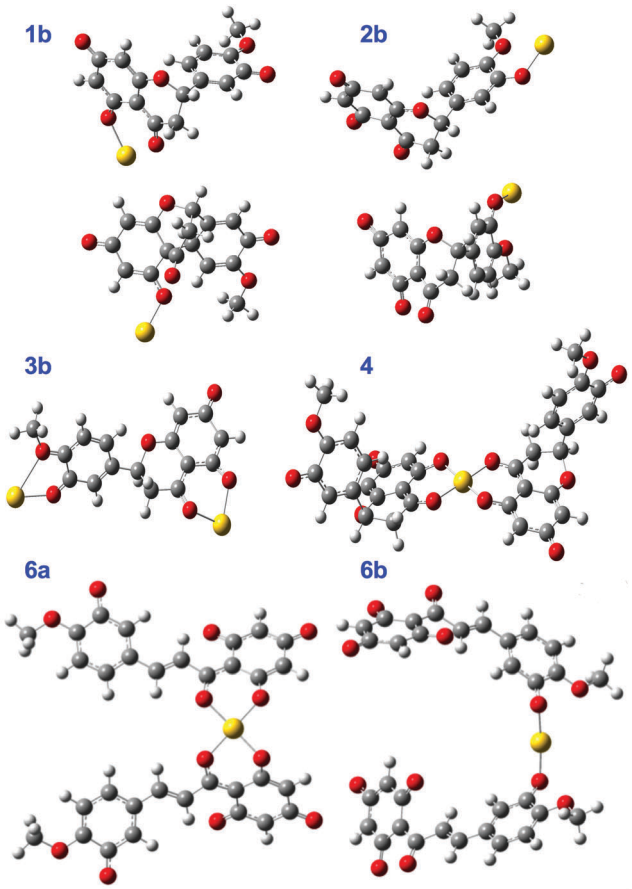

Fig. 8 Final structures of complexes formed in the systems Au^{+3} : Ht^{-3} 1 : 1 1b and 2b, before (upper panel) and after (lower panel) the full geometrical optimization. Followed by structural geometries for Au^{+3} : Ht^{-3} at ratios 2 : 1 (system 3b) and 1 : 2 (system 4). And finally the geometries for the four-fold coordination system 6a and the two-fold coordination system 6b of the Au^{+3}:2Hc^{-4} interactions.

When two Au^{+3} atoms were set to interact with one molecule of Ht^{-3} (system 3b), there was just one situation in which each Au atom interacted either with the two oxygen atoms from the B ring or the two neighboring oxygen atoms from carbonyl and hydroxyl groups in positions C_4 and C_5. The final structural model is shown in Fig. 8. This is an interesting configuration because of the gold atom positions and the distortion of the Ht^{-3} molecule. The interaction is quite strong, as inferred from the formation energy of -15.62 eV. This situation would reflect the interaction of one molecule with a crystallographic plane of the AuNP (two contacts of the Ht molecule with Au atoms) in the capping of the HtAuNPs. The final geometrical configuration in solvent shows Au–O bonds of 2.92 Å/2.17 Å and 2.16 Å/2.11 Å for each coordination site. In a similar way, the configuration

Table 1 HOMO–LUMO energies, energy gap, dihedral angle, formation energies and gold Mulliken charges

System	HOMO (a.u.)	LUMO (a.u.)	Gap (eV)	Φ (°)	Formation energy (eV)	Charge$_{Au}$
Au^{+3} + Ht^{-3} (Gas) (1a)	−0.246	−0.162	2.29	—	−9.90	0.392
Au^{+3} + Ht^{-3} (PCM) (1b)	−0.233	−0.120	3.09	—	−7.91	0.606
Au^{+3} + Ht^{-3} (Gas) (2a)	−0.231	−0.151	2.20	83.54	−9.89	0.289
Au^{+3} + Ht^{-3} (PCM) (2b)	−0.215	−0.186	0.79	56.49	−7.86	0.623
$2Au^{+3}$ + Ht^{-3} (Gas) (3a)	−0.562	−0.543	0.52	−39.76	−18.64	0.786/0.618
$2Au^{+3}$ + Ht^{-3} (PCM) (3b)	−0.267	−0.227	1.09	−36.99	−15.62	0.817/0.872
Au^{+3} + $2Ht^{-3}$ (PCM) (4)	−0.166	−0.120	1.26	97.33	−7.96	0.947
Au^{+3} + Hc^{-4} (PCM) (5)	Molecule fragmentation					
Au^{+3} + $2Hc^{-4}$ (PCM) (6a)	−0.165	−0.094	1.94	−17.87	−218.0	0.834
Au^{+3} + $2Hc^{-4}$ (PCM) (6b)	−0.155	−0.145	0.28	34.56	−217.4	0.277
$2Au^{+3}$ + Hc^{-4} (PCM) (7)	Molecule fragmentation					

calculated for the 1 : 2 ratio of Au : Ht interactions (system 4) displayed Au–O atomic distances of 2.014, 2.008, 2.014 and 2.008 Å, consistent with usual square planar geometry expected for Au^{+3} ions.[53] The hypothesis of the reduction of gold cations by charge transfer from Ht with the further formation of nanoparticles is validated since the final Mulliken charges for gold were again close to zero, see Table 1.[52]

Au^{+3} and charged hesperetin chalcone (Hc^{-4}). The Au : Hc interactions for 1 : 1 (system 5), 1 : 2 (System 6) and 2 : 1 (system 7) ratios were assessed. Because the net charge of Hc is higher −4, compared to −3 for Ht phenolate, the Au:Hc complexes were more stable in water than in the gas phase, and thus only the PCM calculations were performed.

In two specific cases, Au : Hc interacting at 1 : 1 and 2 : 1 ratios, the geometric optimization leads to an important distortions on the Hc molecule. These distortions were significant for considering the molecular fragmentation. The only case where the original Hc geometry remained preserved was for the Au : Hc ratio of 1 : 2 (system 6). Six different configurations were evaluated for an initial four-fold coordination among the O and Au atoms. The most stable configuration (system 6a) displayed fourfold coordination with two oxygen atoms of carbonyl on C1 and the deprotonated hydroxyl on C2 of the 2,4,6-trihydroxyphenyl group, see Fig. 8. This configuration is followed in energy by two-fold geometry coordination, system 6b, a double bidentate coordination, with the oxygen of the hydroxyl from the 3-hydroxy-4-methoxyphenyl group of each Hc molecule; the methoxy group was repelled and moved away from the coordination site. The energy of this configuration (system 6b) is *ca.* 0.72 eV higher in energy terms when compared to the most stable configuration (system 6a). Nevertheless, both situations are still possible; given its highly negative values of formation energies *ca.* −217 eV. This result is a consequence of the negative charge (−4) of the Hc at the selected pH. Regarding the charge distribution, similar results in comparison to Ht were obtained. The atomic charges at Au atoms according to the Mulliken population analysis were +0.834 and +0.277 for systems 6a and 6b, respectively, being quite close those obtained ones for Ht and similar systems.[52]

Despite its limitations TDDFT calculations are a useful one-electron model for understanding the optical spectra of transition-metal complexes, this dealt with the possible experimental characterization predicting the optical absorption in the experimental UV-Vis. For the Au^{3+} : Ht^{-3} 1 : 1 stable structure of complex 2b, the most prominent absorption band was located at 1088 nm, 1029 nm, 801 nm, 539 nm and 441. The most probable electronic transitions having the corresponding

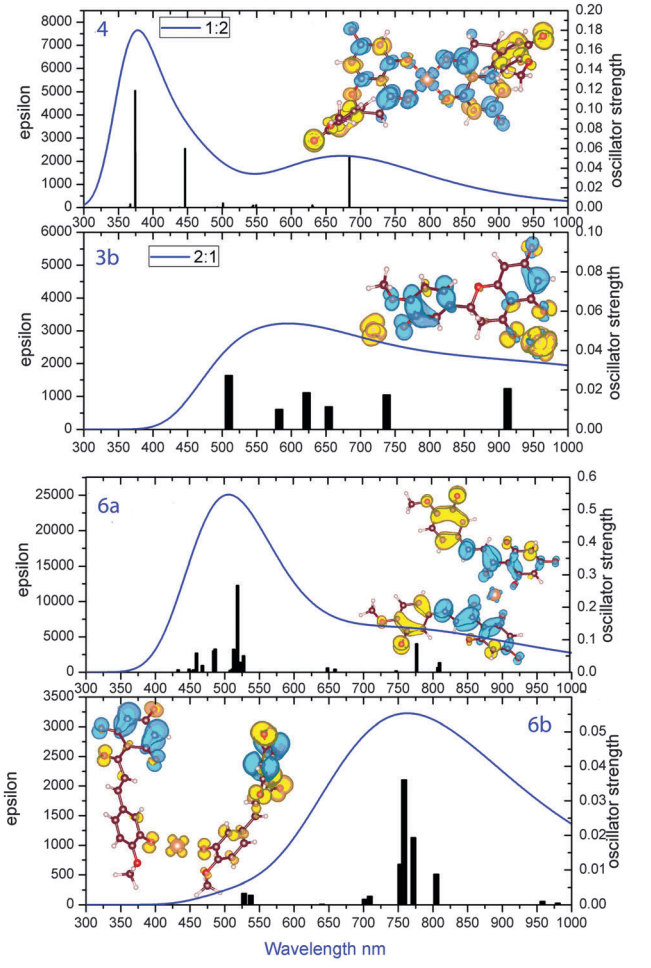

Fig. 9 Optical spectra and electronic density difference maps (EDDM) between the ground state and the most "*f*" intense excited state for Au^{+3} : Ht^{-3} 1 : 2 (system 4) and 2 : 1 (system 3b) and Au^{+3} : Hc^{-4} 1 : 2, (systems 6a and 6b). (*) Excited charge density is represented in cyan and the ground state density is represented in yellow. The iso-density surface is obtained at 0.0002 au. The quantity epsilon stands for the molar absorption coefficient proportional to the imaginary part of the dielectric constant.

vertical excitation and oscillator strengths (f) calculated are reported in Table S2 (ESI†). For the systems $Au^{+3}:Ht^{-3}$ 1:2 and 2:1 the optical properties are shown in Fig. 9, and the tabulated data are available in ESI,† Tables S3 and S4. For $Au^{3+}:Ht^{-3}$ at 1:2 ratio, all transitions are located within the interval 374–684 nm. In this case the transitions are characterized by single and mixed ligand to metal charge transfer (LMCT) and intra ligand charge transfer (ILCT). The most relevant transitions display *f* values up to 0.119. In the case of the $Au^{3+}:Ht^{-3}$ 2:1 ratio, all the transitions were characterized by mixed metal to ligand charge transfer (MLCT) and intra ligand charge transfer (ILCT), and within the interval from 509 to 1071 nm. It is noteworthy that all the relevant transitions present small oscillator strength *f*, which are down to 0.027 or below.

Finally, the TDDFT calculations for two molecules of Hc anions interacting with Au^{+3} show that its optical properties are highly dependent on the Hc–Au coordination. In system 6a the main absorption is located at 500 nm, while in system 6b the main absorption is located at 750 nm (see Fig. 9). Tabulated data with the main contributions are presented in ESI,† Tables S5 and S6.

How experimental and DFT calculations correlate? Experimentally, we have synthetized self-stabilized gold nanoparticles using hesperetin as the reducing agent and by performing quantum chemical calculations using density functional theory (DFT), evidence was obtained that electrons are transferred from hesperetin/chalcone to Au^{3+} ions that are reduced to zero valent gold as a consequence of complexation. For Au:Hc interaction, the fragmentation of the molecule was predicted, giving a reasonable explanation to the appearance of the carboxylate at the HtAuNP film, as determined by XPS. The optical properties expected from TDDFT calculations, system 4 in Fig. 9, are in agreement with the experimental spectrum taken at 0.5 min in Fig. 4a where a λ_{max} around 650 nm was found, thus the gold–hesperetin complex formation could also explain the color for the initial black suspensions.

Conclusions

Here we demonstrated the feasibility to generate stable suspensions of gold nanoparticles using citrus flavonoids under alkaline conditions acting as both reducing and stabilizing agents using the flavonoid hesperetin as the model. Under optimal conditions, hesperetin and its oxidation products provide an effective capping and prevent nanoparticle aggregation without the need for additional stabilizing agents. Unlike all reported biogenic approaches using citrus juices and extracts, this synthetic method uses an isolated molecule from citrus peels, which act as a non-toxic reducing agent in aqueous solution and yields nanoparticles at room temperature with highly reproducible sizes. Using computational simulations the hydroxyl groups involved in the reduction of gold were also shown. Charged species of hesperetin strongly interact with Au^{+3} cations, producing a net charge transfer inducing an electrochemical reduction of gold. It is possible to obtain stable configurations for 1:2 and 2:1 gold to hesperetin ratios, confirming the reduction, and coordination power of this flavonoid. The Time dependent density functional theory calculations support the formation of 1:2 and 2:1 species. Considering that the pH of the starting solutions converts hesperetin into hesperetin chalcone anions, and its reaction with gold was also analyzed. The gold:hesperetin complexes at ratios 2:1 and 1:1 are highly unstable, inducing the fragmentation of the hesperetin chalcone molecule. The gold : hesperetin complexes are stabilized at 1:2 ratio, and the two described situations enable the Au ion reduction by hesperetin chalcone as in the hesperetin case.

Acknowledgements

The authors are in debt to the agencies CAPES, FAPESC, FINEP and CNPQ (Brazil), and PEDECIBA, CSIC, and ANII (Uruguay) for financial support to this work.

References

1 Y. Kim, J. Zhu, B. Yeom, M. Di Prima, X. Su, J.-G. Kim, S. J. Yoo, C. Uher and N. A. Kotov, *Nature*, 2013, **500**, 59–63.
2 C.-J. Jia and F. Schüth, *Phys. Chem. Chem. Phys.*, 2011, **13**, 2457–2487.
3 J. L. Ferry, P. Craig, C. Hexel, P. Sisco, R. Frey, P. L. Pennington, M. H. Fulton, I. G. Scott, A. W. Decho, S. Kashiwada, C. J. Murphy and T. J. Shaw, *Nat. Nanotechnol.*, 2009, **4**, 441–444.
4 M. Kodiha, Y. M. Wang, E. Hutter, D. Maysinger and U. Stochaj, *Theranostics*, 2015, **5**, 357–370.
5 M. Rai, A. P. Ingle, I. Gupta and A. Brandelli, *Int. J. Pharm.*, 2015, DOI: 10.1016/j.ijpharm.2015.10.059.
6 J. Johnston and M. Richardson, *Victoria Univ.*, 2008, **1**, 712–715.
7 A. Patel, P. Prajapati and R. Boghra, *Asian J. Pharm. Clin. Res.*, 2011, **1**, 40–55.
8 C. Li, D. Li, G. Wan, J. Xu and W. Hou, *Nanoscale Res. Lett.*, 2011, **6**, 440.
9 M. Wuithschick, B. Paul, R. Bienert, A. Sarfraz, U. Vainio, M. Sztucki, R. Kraehnert, P. Strasser, K. Rademann, F. Emmerling and J. Polte, *Chem. Mater.*, 2013, **25**, 4679–4689.
10 J. Turkevich, P. C. Stevenson and J. Hillier, *Discuss. Faraday Soc.*, 1951, **11**, 55–75.
11 K. B. Narayanan and N. Sakthivel, *Adv. Colloid Interface Sci.*, 2011, **169**, 59–79.
12 Y. Tai, N. T. T. Tran, Y.-C. Tsai, J.-Y. Fang and L.-W. Chang, *IET Nanobiotechnol.*, 2011, **5**, 52.
13 M. V Sujitha and S. Kannan, *Spectrochim. Acta, Part A*, 2013, **102**, 15–23.
14 N. Basavegowda and Y. Rok Lee, *Mater. Lett.*, 2013, **109**, 31–33.
15 N. Arooj, N. Dar and Z. Q. Samra, *Biomed. Environ. Sci.*, 2014, **27**, 815–818.
16 T. C. Prathna, N. Chandrasekaran, A. M. Raichur and A. Mukherjee, *Colloids Surf., B*, 2011, **82**, 152–159.

17 T. C. Prathna, A. M. Raichur, N. Chandrasekaran and A. Mukherjee, *Proc. Natl. Acad. Sci., India, Sect. B*, 2013, **84**, 65–70.
18 S. Kaviya, J. Santhanalakshmi, B. Viswanathan, J. Muthumary and K. Srinivasan, *Spectrochim. Acta, Part A*, 2011, **79**, 594–598.
19 P. Dauthal and M. Mukhopadhyay, *Korean J. Chem. Eng.*, 2015, **32**, 837–844.
20 E. D. B. Santos, N. V. Madalossi, F. A. Sigoli and I. O. Mazali, *New J. Chem.*, 2015, **39**, 2839–2846.
21 S. Shende, A. P. Ingle, A. Gade and M. Rai, *World J. Microbiol. Biotechnol.*, 2015, **31**, 865–873.
22 V. Nolasco-Arizmendi, R. Morales-Luckie, V. Sanchez-Mendieta, J. Hinnestroza, E. Castro-Longoria and a. R. Vilchis-Nestor, *Text. Res. J.*, 2012, **83**, 1229–1235.
23 D. P. Pavarini, S. P. Pavarini, M. Niehues and N. P. Lopes, *Anim. Feed Sci. Technol.*, 2012, **176**, 5–16.
24 L. Gobbo-neto and N. P. Lopes, *Quim. Nova*, 2007, **30**, 374–381.
25 T. C. Prathna, M. Lazar, N. Chandrasekaran and A. M. Raichur, in *Biomimetics Learning from Nature*, ed. A. Mukherjee, InTech, 2010.
26 A. Roohbakhsh, H. Parhiz, F. Soltani, R. Rezaee and M. Iranshahi, *Life Sci.*, 2014, **113**, 1–6.
27 J. Londoño-Londoño, V. R. De Lima, O. Lara, A. Gil, T. B. C. Pasa, G. J. Arango and J. R. R. Pineda, *Food Chem.*, 2010, **119**, 81–87.
28 C. a Schneider, W. S. Rasband and K. W. Eliceiri, *Nat. Methods*, 2012, **9**, 671–675.
29 W. Kohn and L. J. Sham, *Phys. Rev.*, 1965, **140**, A1133–A1138.
30 P. Hohenberg and W. Kohn, *Phys. Rev.*, 1964, **136**, B864–B871.
31 M. J. Frisch, G. W. Trucks, H. B. Schlegel, G. E. Scuseria, M. A. Robb, J. R. Cheeseman, G. Scalmani, V. Barone, B. Mennucci, G. A. Petersson, H. Nakatsuji, M. Caricato, X. Li, H. P. Hratchian, A. F. Izmaylov, J. Bloino, G. Zheng, J. L. Sonnenberg, M. Hada, M. Ehara, K. Toyota, R. Fukuda, J. Hasegawa, M. Ishida, T. Nakajima, Y. Honda, O. Kitao, H. Nakai, T. Vreven, J. A. Montgomery, Jr., J. E. Peralta, F. Ogliaro, M. Bearpark, J. J. Heyd, E. Brothers, K. N. Kudin, V. N. Staroverov, R. Kobayashi, J. Normand, K. Raghavachari, A. Rendell, J. C. Burant, S. S. Iyengar, J. Tomasi, M. Cossi, N. Rega, J. M. Millam, M. Klene, J. E. Knox, J. B. Cross, V. Bakken, C. Adamo, J. Jaramillo, R. Gomperts, R. E. Stratmann, O. Yazyev, A. J. Austin, R. Cammi, C. Pomelli, J. Ochterski, R. L. Martin, K. Morokuma, V. G. Zakrzewski, G. A. Voth, P. Salvador, J. J. Dannenberg, S. Dapprich, A. D. Daniels, O. Farkas, J. B. Foresman, J. V. Ortiz, J. Cioslowski and D. J. Fox, *GAUSSIAN 09 (Revision A.02)*, Gaussian, Inc., Wallingford, CT, 2009.
32 R. G. Parr and W. Yang, *Density-functional theory of atoms and molecules*, Oxford University Press, Oxford, 1989.
33 A. D. Becke, *J. Chem. Phys.*, 1993, **98**, 5648–5652.
34 J. P. Perdew, K. A. Jackson, M. R. Pederson, D. J. Singh and C. Fiolhais, *Phys. Rev. B: Condens. Matter Mater. Phys.*, 1992, **46**, 6671–6687.
35 P. J. Hay and W. R. Wadt, *J. Chem. Phys.*, 1985, **82**, 270–283.
36 B. Mennucci and J. Tomasi, *J. Chem. Phys.*, 1997, **106**, 5151.
37 E. Runge and E. K. Gross, *Phys. Rev. Lett.*, 1984, **52**, 997–1000.
38 R. Bauernschmitt and R. Ahlrichs, *Chem. Phys. Lett.*, 1996, **256**, 454–464.
39 M. Scampicchio, J. Wang, A. J. Blasco, A. Sanchez Arribas, S. Mannino and A. Escarpa, *Anal. Chem.*, 2006, **78**, 2060–2063.
40 S. Das, P. Roy, S. Mondal, T. Bera and A. Mukherjee, *Colloids Surf., B*, 2013, **107**, 27–34.
41 B. Streszewski, W. Jaworski, K. Pacławski, E. Csapó and I. Dékány, *Colloids Surf., A*, 2012, **397**, 63–72.
42 G. Gattuso, D. Barreca, C. Gargiulli, U. Leuzzi and C. Caristi, *Molecules*, 2007, **12**, 1641–1673.
43 G. Milczarek and A. Ciszewski, *Colloids Surf., B*, 2012, **90**, 53–57.
44 Y. Mikhlin, A. Karacharov, M. Likhatski, T. Podlipskaya, Y. Zubavichus, A. Veligzhanin and V. Zaikovski, *J. Colloid Interface Sci.*, 2011, **362**, 330–336.
45 R. Wallace, A. P. Brown, R. Brydson, S. J. Milne, N. Hondow and P. Wang, *J. Phys.: Conf. Ser.*, 2012, **371**, 012080.
46 D. Mahl, J. Diendorf, W. Meyer-Zaika and M. Epple, *Colloids Surf., A*, 2011, **377**, 386–392.
47 M. R. Ivanov, *PhD Thesis*, University of Iowa, 2011.
48 S. K. Balasubramanian, L. Yang, L.-Y. L. Yung, C.-N. Ong, W.-Y. Ong and L. E. Yu, *Biomaterials*, 2010, **31**, 9023–9030.
49 M. R. Ivanov, H. R. Bednar and A. J. Haes, *ACS Nano*, 2009, **3**, 386–394.
50 T. Herranz, X. Deng, A. Cabot, P. Alivisatos, Z. Liu, G. Soler-Illia and M. Salmeron, *Catal. Today*, 2009, **143**, 158–166.
51 A. Di Mauro, B. Fallico, A. Passerini, P. Rapisarda and E. Maccarone, *J. Agric. Food Chem.*, 1999, **47**, 4391–4397.
52 D. K. Singh, R. Jagannathan, P. Khandelwal, P. M. Abraham and P. Poddar, *Nanoscale*, 2013, **5**, 1882–1893.
53 W. R. Mason and H. B. Gray, *Inorg. Chem.*, 1968, **7**, 1963–1966.